In situ laser reflectivity to monitor and control the nucleation and growth of atomically-thin 2D materials

To cite this article before publication: Alexander A. Puretzky *et al* 2020 *2D Mater.* in press https://doi.org/10.1088/2053-1583/ab7a72

In situ laser reflectivity to monitor and control the nucleation and growth of atomically-thin 2D materials

Alexander A. Puretzky[1]*, Yu-Chuan Lin[1], Chenze Liu[2], Alex M. Strasser[3], Yiling Yu[1], Stela Canulescu[4], Christopher M. Rouleau[1], Kai Xiao[1], Gerd Duscher[2], David B. Geohegan*[1]

[1] *Center for Nanophase Materials Sciences, Oak Ridge National Laboratory, Oak Ridge 37831*
[2] *Department of Materials Science and Engineering, University of Tennessee, Knoxville 37996*
[3] *Artie McFerrin Department of Chemical Engineering, Texas A&M University, College Station, TX 77843*
[4] *Department of Photonics Engineering, Technical University of Denmark, Lyngby, Denmark*

Abstract

The growth of atomically-thin two-dimensional (2D) layered and other quantum materials is typically performed without *in situ* monitoring or control. Here, a simple laser reflectivity approach is demonstrated to provide *in situ* control over sub-monolayer thickness and growth kinetics during pulsed laser deposition (PLD) of $MoSe_2$ layers. First, the general technique is presented with emphasis on designing the maximum sensitivity of the optical contrast through consideration of Fresnel's equations with proper choice of layer thickness, substrate, and laser monitoring wavelength, incidence angle, and laser polarization. Then the 633 nm optical reflectivity of $MoSe_2$ layers on SiO_2/Si substrates was predicted and compared with *in situ* monitoring of $MoSe_2$ growth by PLD under actual growth conditions using a probe HeNe laser beam. The measurements showed high sensitivity and excellent agreement with $MoSe_2$ surface coverages calculated from atomic resolution STEM analysis of 2D layers deposited in arrested growth experiments. Growth kinetics revealed by these measurements showed sigmoidal nucleation and growth stages in the formation of the 2D $MoSe_2$ layers that are described by a simple model, indicating the promise of the laser reflectivity technique for *in situ* monitoring and control of 2D materials deposition.

Keywords: *in situ* reflectivity, pulsed laser deposition (PLD), 2D materials, $MoSe_2$, kinetic modeling

Introduction

The lack of simple diagnostics for measuring the nucleation and growth kinetics of atomically-thin layered 2D materials and other quantum materials is hindering their rational development. In addition, practical methods are needed for routine *in situ* diagnostic monitoring and control of growth parameters. This is partly due to the high-temperature environment and closed nature of tube furnaces and common vacuum systems used for 2D materials growth that preclude the adoption of optical techniques such as *in situ* spectroscopic ellipsometry, which has been used as the method of choice to monitor and control the growth of ultrathin films by atomic layer deposition.[1-3]

With simplicity and versatility in mind for applicability in the broadest variety of growth reactors used for 2D materials, here we describe and apply a single-wavelength laser reflectivity technique for *in situ* monitoring of layered materials growth. We apply the technique to understand the nucleation and growth of $MoSe_2$ films during pulsed laser deposition (PLD) in vacuum. PLD is an emerging technique for the synthesis of atomically-thin, layered 2D materials that naturally allows digital control of the deposition rate [4], with material typically arriving to the substrate just microseconds after each laser pulse. In a typical PLD experiment a pulsed laser (~25 ns, 248 nm, ~ 1 J/cm^2) irradiates a solid target, creating a plasma plume that transports precursors nearly stoichiometrically to a heated substrate (Fig.1(a)) with a distribution of velocities that are typically maximize at ~ 1 cm/μs in vacuum, corresponding to kinetic energies of 40-50 eV/atom for either Mo or Se. The plasma plumes can penetrate background gases that can be employed to moderate the kinetic energies of the ablated species, effect reactive chemistry, or induce condensation of

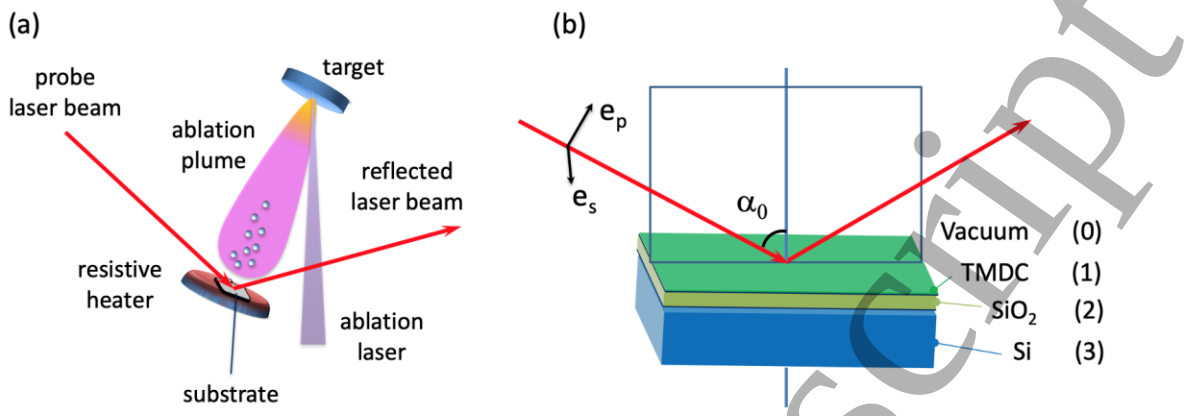

Figure 1. (a) Schematic of a typical pulsed laser deposition setup for layered 2D materials with *in situ* laser reflectivity diagnostics. (b) An example of a bilayer system that includes a variable number of transition metal dichalcogenide (TMDC) layers and a thin layer of SiO_2 on a Si substrate along with an incident laser with s- and p-polarizations (left).

atoms and molecules into clusters and nanoparticles. [4-6] Upon successive laser plasma pulses colliding with the substrate, the precursors tend to form a uniform thin film e.g., a single- or multi-layer transition metal dichalcogenide (TMDC) film. The nucleation density is typically high, leading to uniform films over ~ 1 cm^2 area, which is an advantage over chemical vapor deposition (CVD) approaches in tube furnaces. However, both growth approaches are very sensitive to deposition conditions and require *in situ* diagnostics to understand and control the nucleation and growth processes.

Can the nucleation and growth kinetics of atomically-thin 2D materials be monitored using laser reflectometry using a single wavelength? This approach has been used successfully in the past for monitoring the deposition of thicker films during PLD [7-11], and as we have shown recently, this approach has been very useful for understanding the growth kinetics and mechanisms of vertically aligned carbon nanotubes[12-16] and graphene (on Ni foils)[17, 18] synthesis by CVD. However, monitoring the synthesis of atomically-thin films is somewhat challenging because it requires optimization of the optical contrast between the material of choice and the underlying combination of layers and substrates, (e.g., SiO_2, $MoSe_2$ and Si as shown in Fig. 1(b)).

Optimization of such an apparently simple system requires the careful consideration of several variables such as the laser probe wavelength, its incidence angle and polarization, and the thickness of the SiO_2 layer. Although similar considerations have been presented to optimize the visualization of graphene [19-23], black phosphorous [24, 25], TMDCs [26, 27], and other 2D materials using optical microscopes (see Review [28]), a general analysis applicable for *in situ* single-wavelength laser reflectometry of 2D material growth in typical growth reactors has not been considered. Here, we provide a detailed description of this problem that allows choosing the optimal experimental parameters for *in situ* monitoring of 2D materials growth and the sensitive measurement of their nucleation and growth kinetics by PLD or CVD approaches.

Results and discussions

Optimization of SiO_2 layer thickness for different 2D materials

Calculating the optical characteristics of a stack of layers has long been established using a number of mathematical approaches based on Fresnel's equations, the most common of which being the recursive and transfer-matrix methods [29]. The recursive approach is based on an effective layer approximation to remove successive layers starting from the bottom. This approach follows a methodology that replaces the amplitudes of the reflection and transmission coefficients of a pair of layers (e.g., layers 2 and 3 in Fig. 1(b)) with that of a single effective layer. Then, that effective layer is combined with the next layer in the stack, and so on. This contrasts with the transfer-matrix approach where the reflectance and transmission from a stack of layers can be treated as the product of matrices corresponding to each individual layer [29]. Following the recursive approach, the reflection and transmission of s- and p-polarized light from a stack of homogeneous layers can be calculated using the incidence angle, α_0, and amplitude reflection, r_i,

and transmission, t_i, coefficients of individual layers, where $i = 0, 1, \ldots n$ and $\tilde{n}_i = n_i - ik_i$ is the complex refractive index for each layer (n_i is the refractive index and k_i is the extinction coefficient) (see details in the Supporting Information (SI): section S1, Eq. S3). The reflection coefficient of a two-layer stack on a substrate in vacuum ($n_0 = 1$) or in ambient gas can then be determined as

$$R_{s,p} = \left|r_{s,p}\right|^2 \qquad (1)$$

Where the appropriate $r_{i,i+1}$ should be used for s- or p-polarized light (Eqs. S1a-c) in (Eq. S3).

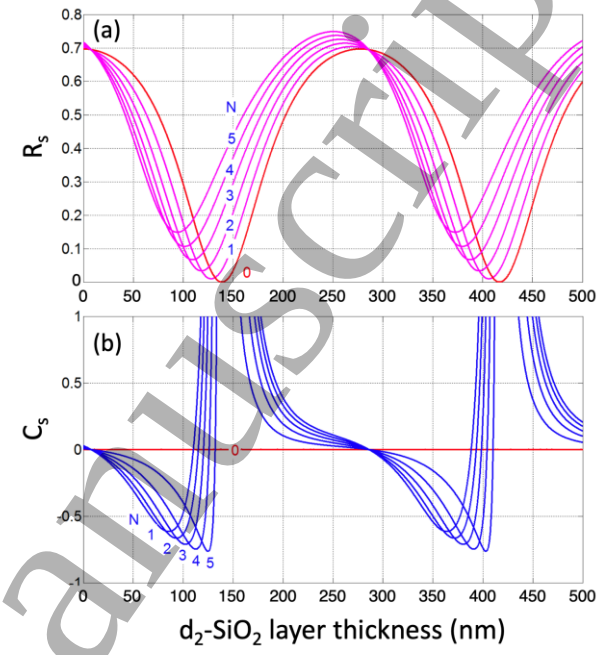

Figure 2. (a) Reflected intensity, R_s, and (b) contrast, C_s, versus the thickness of the SiO_2 layer for s-polarized laser light calculated for different numbers of $MoSe_2$ layers, N, from 1 to 5 with the thickness of an individual layer equal to 0.65 nm. The red lines correspond to the reflection from the bare SiO_2/Si stack. The laser wavelength is 632.8 nm with the incidence angle α_0= 70°. The following refractive indices are used in the calculations: n_0=1 (vacuum); $\tilde{n}_1$=4.70-1.06i ($MoSe_2$ [30]); n_2=1.48 (SiO_2); and $\tilde{n}_3$=3.87-0.016i (Si [31]).

While the thickness of the SiO_2 layer, d_2, determines the main interference fringes in the reflected light intensity, the atomically thin TMDC layers provide a small, but important perturbation to the interference patterns that should be optimized to achieve the highest relative contrast, $C_{s,p} = (R_{s,p} - R_{s,p0})/ R_{s,p0}$, compared to the reflectivity of the stack without TMDC layers denoted by the subscript 0, $R_{s,p0}$. The calculated reflected intensities and contrasts for different numbers of $MoSe_2$ layers, N, from 1 to 5 in the case of s-polarized light are shown in Figs. 2(a) and 2(b) respectively together with the reflectivity from a bare SiO_2/Si stack. In this case, we choose the 632.8 nm HeNe-laser wavelength for optical reflectivity, and the calculations were conducted using Matlab. Note that these calculations utilize idealized optical surfaces that result in zero reflectivity for the specific

thicknesses of the SiO_2 layers for which the contrast, C_s, cannot be defined. From these calculations we can make the following important conclusions for choosing the optimal substrates for *in situ* monitoring of TMDC deposition. 1) The thickness of the SiO_2 layer should be in the range of 85-125 nm, and 2) The SiO_2 thickness should be adjusted to optimize the monitoring of specific numbers of TMDC layers, e.g., 85 nm should be chosen for N=1 and 125 nm for N=5. Note that arbitrarily choosing a SiO_2 thickness of ~300 nm that is typically used for optical microscopy of graphene [19-23] will lead to almost zero contrast and therefore, no changes in the reflected intensity upon TMDC film deposition would be observable at the specified incidence angle and the laser wavelength. This indicates the critical role of the SiO_2 thickness parameter for optical reflectivity probing of the TMDC film deposition, i.e., the right choice of the SiO_2 layer thickness gives a remarkably large contrast,$|C_s|$=0.61 for N=1 using the considered parameters (see the caption to Fig. 2).

We consider now the case of p-polarized light while keeping all other parameters the same as in the s-polarization case. Figure 3 shows the calculated reflected intensities, R_p, and contrasts, C_p, for different numbers of $MoSe_2$ layers from 1 to 5. In this case, zero contrast for all five considered layers is observed at the SiO_2 thicknesses of 217 nm and 288 nm and a maximum contrast, $|C_p|$ =0.13 is calculated for a single $MoSe_2$ layer at d_2=32 nm, which is considerably smaller than that for the case of s-polarized light. Therefore, p-polarized laser light does not provide a good contrast for *in situ* monitoring of TMDC film deposition. However, in the case of p-polarization the contrast shows much weaker dependence on the SiO_2 layer thickness compared to that for s-polarization. A possible strategy to combine the advantages of probing with s- and p-polarized light is to use randomly polarized light. To analyze this option, we calculated the contrast, C_r, which is shown in Figs. 4(a) and 4(b). One can see that in this case the contrast is less

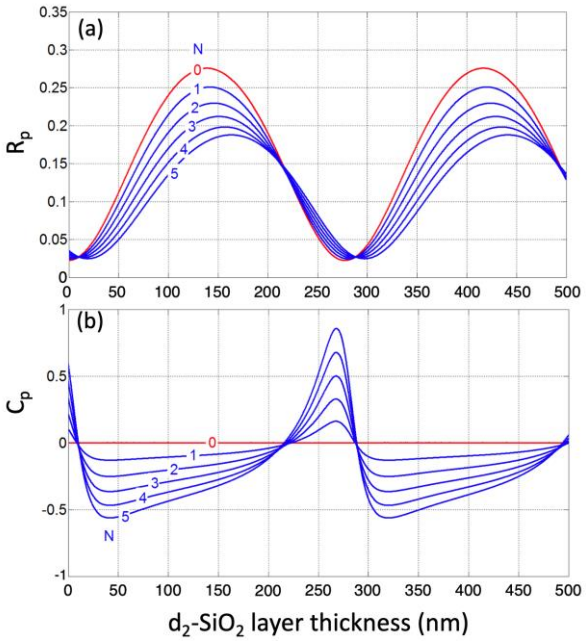

Figure 3. (a) Reflected intensity, R_p, and (b) contrast, C_p, versus the thickness of the SiO_2 layer for p-polarized laser light calculated for different numbers of $MoSe_2$ layers, N, from 1 to 5 with the thickness of an individual layer equal to 0.65 nm. The red lines correspond to the reflection from the bare SiO_2/Si stack without the $MoSe_2$ layers. The laser wavelength is 632.8 nm with the incidence angle α_0=70°. All other parameters are identical to those described in the caption of Fig. 2.

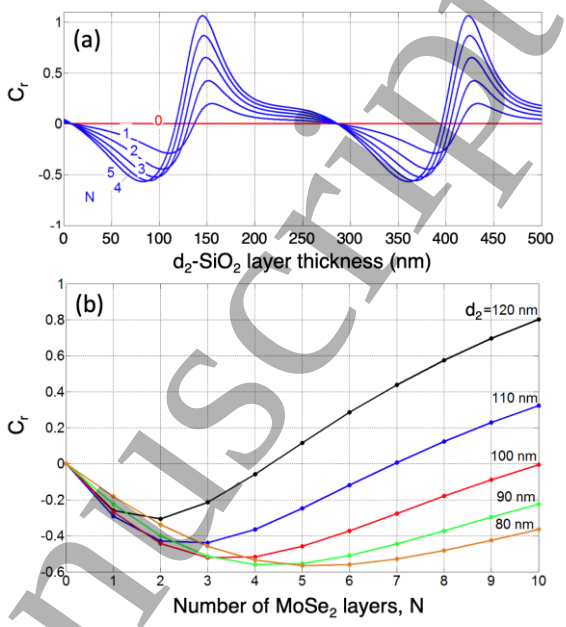

Figure 4. (a) Contrast, C_r, versus the thickness of the SiO_2 layer for randomly polarized laser light calculated for different number of $MoSe_2$ layers, N, from 1 to 5 with the thickness of an individual layer equal to 0.65 nm. The laser wavelength is 632.8 nm with the incidence angle α_0=70°. All other parameters are identical to those described in the caption of Fig. 2. (b) C_r versus number of $MoSe_2$ layers with different thicknesses of the SiO_2 layer from 80 to 120 nm.

sensitive to the thickness of the SiO_2 layer compared to that for s-polarized light and still shows appreciable values. For example, in the case of a single $MoSe_2$ layer $|C_r|$ = 0.25 (d_2=110 nm) and changes to 0.57 (d_2=80 nm) for N=5. Similar to the other two cases for polarized light, zero contrast is still observed for some specific values of d_2.

Another important point that should be considered for *in situ* monitoring of TMDC films deposition is the relative contrast of the sequential layers. For example, from Fig. 4(b) one can see that the contrast is not usually a linear function of the number of layers and exhibits minima at different N depending on the thickness of the SiO_2 layer, d_2, with almost no relative contrast

between the mutual layers near the minima. Therefore, for monitoring of few layer TMDC films, the SiO_2 layer thickness can be chosen to give an approximately linear change in reflectivity or contrast. For example, choosing d_2 =80 nm (Fig. 4(b)) provides an approximately linear change of contrast for up to 4 layers, but with the absolute contrast value for a single layer dropping to 0.18. The minima in the contrast versus the number of layers (Fig. 4(b)) also can provide a good *in situ* indication of TMDC layer numbers as will be discussed below.

Choice of incidence angle

In many cases the choice of the incidence angle of the laser with the substrate is determined by the constraints of the experimental setup used for PLD or CVD. For example, our PLD chamber (Fig. S6) required an oblique incidence angle of 78°. However, in cases when this restriction does not exist the choice of an optimal incidence angle can result in a substantial increase of the absolute value of the contrast, C_r. Figure 5 shows the dependence of C_r on incidence angle calculated for a single $MoSe_2$ layer and different thicknesses of the SiO_2 layer from 80 nm to 120 nm. One can see that at oblique incidence angles the contrast weakly depends on the thickness of the SiO_2 layer. However, much stronger dependence is observed at smaller incidence angles from 0° to ~30°. In this case, choosing d_2=90 nm along with 10° angle of incidence, for example, will result in an absolute

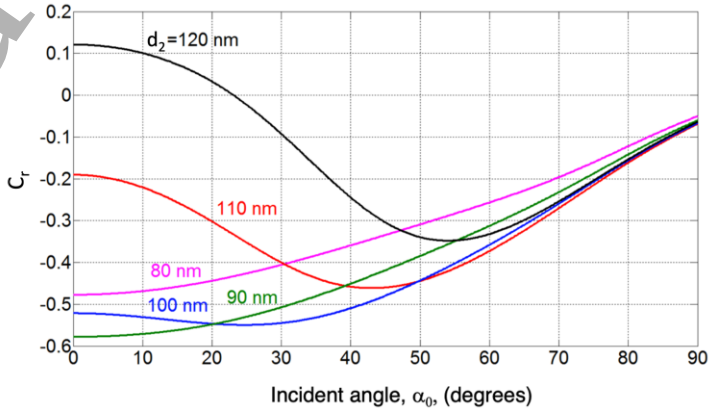

Figure 5. Contrast, C_r, versus incidence angle, α_0, for randomly polarized laser light calculated for a $MoSe_2$ monolayer (N=1) and different thicknesses of the SiO_2 layer from 80 to 120 nm. All other parameters are identical to those described in the caption of Fig. 2.

value of contrast equal to 0.57, which is approximately 2 times larger than that for a 70° angle of incidence.

Choice of laser wavelength

Analysis of the wavelength dependence of the contrast is more challenging since it requires knowledge of $\tilde{n}_i(\lambda)$. Here, we used $\tilde{n}_1(\lambda)$ for a $MoSe_2$ monolayer derived from the dielectric functions measured in Ref. [30]. The corresponding $\tilde{n}_1(\lambda)$ are listed in Table 1 together with $\tilde{n}_3(\lambda)$ for Si substrates taken from Ref. [31]. In addition to the previously used HeNe laser wavelength (632.8 nm), we performed contrast calculations at the wavelengths corresponding to the resonances of the excitons A, B, and C of a $MoSe_2$ monolayer. The results of these calculations are shown in Fig. 6, and one can see (see Eq. S4) that the optimal SiO_2 layer thicknesses change for different wavelengths, e.g., from 81 nm

Table 1. Complex refractive indices of $MoSe_2$ monolayer, SiO_2 layer, and Si substrate used for calculations of $C_r(\lambda)$ at the wavelengths corresponding to the excitonic resonances A, B, and C of a $MoSe_2$ monolayer.

λ (nm)	$MoSe_2$ exciton	Layer 1 $MoSe_2$ [30]	Layer 2 SiO_2	Substrate Si [31]
632.8		4.7042-1.0629i	1.4761	3.872-0.01637i
477	C	4.620-3.138i	1.4782	4.428-0.0615i
709	B	4.583-3.464i	1.4705	3.755-0.0094i
826	A	4.80-3.464i	1.4689	3.675-0.0050i

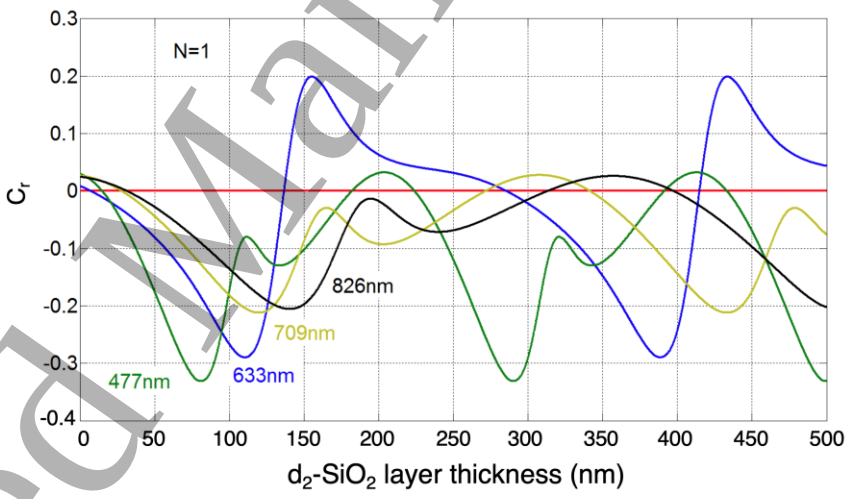

Figure 6. Contrast, C_r, versus the thickness of the SiO_2 layer for randomly polarized laser light calculated for the set of wavelengths corresponding to the excitonic resonances A, B, and C of $MoSe_2$ monolayer. The complex refractive indices used in calculations are listed in Table 1.

(λ= 477 nm) to 142 nm (λ= 826 nm). However, the absolute value of the contrast changes only from 0.33 to 0.21, respectively, for these two wavelengths.

Comparison with experiment

Figures 7(a) and 7(b) give an example of *in situ* reflectivity monitoring of $MoSe_2$ film deposition by PLD. In this case a $MoSe_2$ film was deposited on a SiO_2 (d_2=110 nm)/Si substrate using an excimer laser (KrF, 248 nm, 0.9 J/cm^2, pulse width ~ 25 ns FWHM, 1 Hz repetition rate) ablation in vacuum ($5\cdot10^{-6}$ Torr). The substrate was placed 5 cm from the target and was heated up

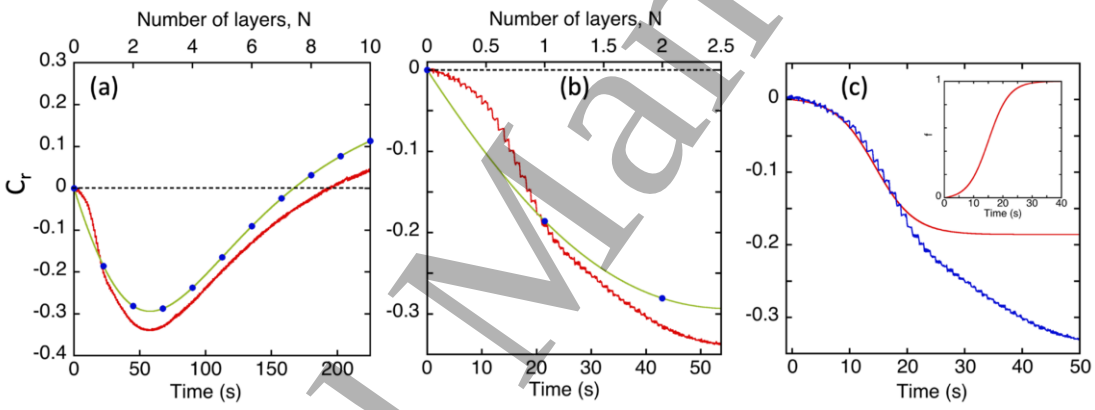

Figure 7. (a) Comparison of the measured reflectivity contrast vs. time (red curves) and calculated C_r reflectivity contrast vs. thickness (blue dots and green curves). Calculations were conducted using $\tilde{n}_i(\lambda)$ listed in Table 1 with d_2=110 nm, λ = 633nm, and incidence angle α_0= 78°. $MoSe_2$ film deposition was performed using an excimer laser (KrF, 248 nm, 0.9 J/cm^2, ~ 25 ns pulse width, 1Hz repetition rate) in vacuum ($5\cdot10^{-6}$ Torr) at a substrate temperature of 600 °C. The calculated and measured C_r minima positions were used to match the growth time with the number of $MoSe_2$ layers. (b) Magnified region showing the onset part of the C_r, and the incremental reflectivity changes upon deposition from each laser pulse (c) A monolayer reflectivity, C_r, fit using Eq. S9 (red curve). The inset shows f(t) used for this fit.

to 600 °C before deposition. A randomly polarized HeNe laser beam (632.8 nm) incident at 78° was used, and the intensity of the incident and reflected beams were monitored using Si photodiodes equipped with 633 nm interference filters. A SourceMeter (Keithley 2400) recorded the photocurrents at 7 samples per second.

To compare and calibrate the predicted C_r versus layer number with the measured C_r versus time, the two curves were plotted together in Figs. 7(a) and 7(b) by scaling the x-axes to match minima positions. If the growth rate was constant (as expected from our constant 1 Hz PLD) and the film grew with perfect adherence to the assumptions of the idealized optical model (discussed below), the two curves should overlap. While the agreement is remarkably good, there are some interesting differences in the growth process that are highlighted in the magnified view of Fig. 7(b). First, during the first 20 laser pulses corresponding to the deposition of ~ 1 monolayer the declinations during each pulse are clearly observable, allowing for submonolayer (digital) control over average thickness (see also section S7). Second, the data indicate a slower growth during a nucleation phase followed by a more accelerated growth, which will be discussed in terms of a growth model below.

To understand how the actual surface coverage of $MoSe_2$ on the substrate varied for different numbers of predicted layers, and to probe the *in situ* ability of laser reflectivity to control the growth process for a given number of layers, a series of stop-growth experiments were conducted using the same conditions (KrF ablation of $MoSe_2$ in vacuum, d = 5 cm, 110-nm-thick SiO_2 on Si substrates held at 600°C). Transmission electron microscopy (TEM) grids made of graphene were attached to the substrates for direct analysis of layer number by atomic resolution Z-contrast scanning TEM (STEM). Four different $MoSe_2$ deposition runs were monitored *in situ* with planned termination after reflectivity declines of 5%, 17%, 22%, and 31%, as shown in Figs. 8(a)-8(d), respectively. After 12 laser pulses (Figs. 8(a), 8(e), and 8(i)) the measured reflectivity decline corresponded to a fractional monolayer coverage of 0.38 according to theoretical predictions, while areal analysis of the monolayer coverage measured from the STEM image was

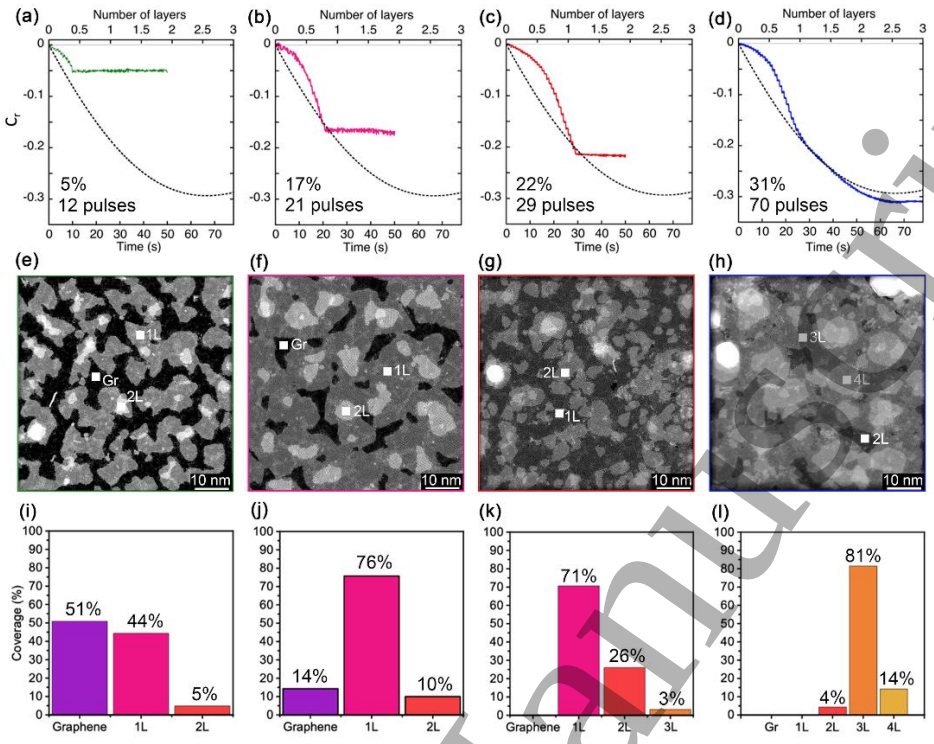

Figure 8. (a)-(d) Measured reflectivity (C_r) curves of a 633nm laser beam during stop-growth PLD experiments that terminate after 12, 21, 29, and 70 laser pulses. The corresponding values of the $|C_r|$ % drops are also listed. The dashed curves indicate calculated C_r, (same as shown in Fig.7(a) and 7(b)) where the calculated and measured minima positions were used to match the growth time with the number of $MoSe_2$ layers. (e)-(h) Atomic resolution STEM images of $MoSe_2$ deposited at the same time on graphene witness grids corresponding to the stop-growth depositions in (a)-(d). (i)-(l) Histograms of layer coverage obtained by analysis of the STEM images (e)-(h) using ImageJ.

0.44. The selected area of the atomic resolution STEM image (Fig. 8(e)) presenting Z-contrast profiles corresponding to the Mo and 2Se atoms is shown in the Supporting Information (section S2, Fig. S1).

Similarly, after 21 laser pulses the measured reflectivity indicated a predicted coverage of 0.8, while the STEM image in Fig. 8(j) showed 0.76 ML coverage, and 0.1 bilayer coverage. After 29 pulses, when a complete monolayer of $MoSe_2$ is predicted, indeed we find that the entire monolayer is nearly filled in addition to there being a 0.26 bilayer fraction. After 70 pulses, corresponding to a predicted 3 layers of $MoSe_2$, we find 0.81 of the film areas is actually 3-layer, while 0.04 is 2-layer, and 0.14 is 4-layer. This comparison shows that this monitoring approach

gives a good estimate of the surface coverage that can be used as a simple and useful tool to control growth of TMDC layers by PLD.

To check the constant growth rate assumption in the considered range of laser pulses (from 12 to 70), we plot the total amount of layered $MoSe_2$ material from the estimates of the surface coverage shown in Figs. 8(a)-8(l) versus the corresponding number of the laser pulses used in each case (Fig. S7). The details of this analysis are described in the section S7 of the Supporting information. We found that in this case the constant growth rate can be used to describe the amount of the deposited material by 12-70 laser pulses. However, the initial phase of the growth ($\lesssim$20 laser pulses) is not linear and cannot be described by the average growth rate. The required consideration of the nucleation stage is addressed below.

To further confirm that PLD of a $MoSe_2$ target results in formation of $MoSe_2$ layers, Raman spectra of the deposited films for a set of the stop-growth experiments were measured (see the SI: section S3, Fig. S2). The Raman spectra (Fig. S2(d)) clearly show emergence of the $A_1'(A_{1g})$ $MoSe_2$ peaks at 240 cm^{-1} for the 17 and 30 laser pulses samples corresponding approximately to a monolayer and a bilayer surface coverage. However, atomic force microscopy (AFM) images of the same stop-growth experiments samples (see the SI: section S4, Fig. S3) did not reveal any $MoSe_2$ regions, likely due to the size of the $MoSe_2$ domains being comparable to the size of the AFM tip (~30 nm) as can be seen from Fig. 8(e).

Growth kinetics

As mentioned above, the steps in the reflected light intensity that are evident in Fig. 7(b) reflect the deposition resulting from each laser pulse. In fact, the fast time response within each reflectivity step contains information about the kinetics of deposition, desorption, and

crystallization following the arrival of material from each ablation plume – the timescales for which can be compared with gated ICCD photography (see an example in the SI: section S5, Fig. S4) and ion probe waveforms of the laser plasma propagation (illustrated schematically in Fig. 1(a)) that will be published elsewhere. From Figs. 7(a) and 7(b), we can estimate that approximately 20-30 laser pulses are required to form a complete monolayer.

However, Fig 7(b) (and all other reflectivity curves) clearly indicate that at the beginning ($\lesssim$20 initial laser pulses) growth does not proceed linearly. Instead, monolayer formation kinetics exhibit sigmoidal behavior revealing a slow nucleation stage followed by more rapid growth, similar to that observed for graphene growth by CVD [18, 32]. Another interesting observation is that upon the reflectivity expected for the completion of the first monolayer the growth kinetics appear to exhibit a kink. To further elaborate the growth kinetics, we consider a simple autocatalytic kinetic model described in our previous work [18], which is also briefly described in the Supporting Information (section S6). In general terms, this model considers a two-step process of conversion of precursor species A to intermediate species B involving nucleation (step 1, Eq. S6a) and growth (step 2, Eq. S6b) reactions with the rate constants, k_n and k_{gr}, respectively.

One possibility that has been considered for graphene growth by CVD in our previous work [32] was based on the interpretation of the kinetic parameters (m_1 and m_2 in Eq. (S8)) in terms of sticking coefficients, s_0 and s_1, of the reactive species that describes their capturing at random vacant sites on a substrate and on the top of formed monolayer crystals, respectively. In this case, the fractional surface coverage, $f(t)$, can be described by the following equation (see section S6 in the SI):

$$f(t) = \frac{\frac{s_0}{s_1}\left(e^{J(s_0+s_1)t}-1\right)}{1+\frac{s_0}{s_1}e^{J(s_0+s_1)t}}, \quad f(0) = 0, \qquad (2)$$

where J is the flux to a single reactive site. Eq. (2) can be used to approximate the experimental reflectivity curves of a monolayer as shown in Fig. 7(c) assuming $N = f(t)$. This fit gives $\frac{s_0}{s_1} = 0.013$ with $\tau = \frac{1}{Js_1} \approx 3.5$ s. This analysis shows that the autocatalytic kinetics, Eq. (2), explains well the initial part of the experimental reflectivity curve corresponding to monolayer growth. The small value of the $\frac{s_0}{s_1}$ indicates the kinetics are limited by the nucleation step.

Interestingly, these experimentally observed nucleation kinetics are very sensitive to the growth conditions. For example, analysis and comparison of the initial growth kinetics in the stop-growth experiments (shown in Fig. S5) indicates that there are noticeable differences among runs despite all the PLD growth parameters having been kept the same. This demonstrates the importance of *in situ* monitoring of the film deposition to control the nucleation step and opens the door to making adjustment of the kinetics to promote controlled nucleation and growth.

Conclusions

Here, we demonstrated a simple *in situ* laser reflectivity approach to monitor and control the deposition of 2D materials that can be used with different deposition techniques. As an example, $MoSe_2$ films were deposited on commonly used Si substrates with thin SiO_2 layers at 600°C by PLD in vacuum. To monitor the deposition of different numbers of $MoSe_2$ layers it is essential that the thickness of the SiO_2 layer be chosen to provide the best optical contrast in conjunction with the laser excitation wavelength, incidence angle, and laser polarization for a particular experimental geometry. By choosing these optimal parameters, the optical reflectivity can serve as a very sensitive tool for *in situ* monitoring of 2D materials deposition.

The agreement between experimental and predicted reflectivity values was surprisingly good, however it is important to note the limitations of the calculations. First, ideal stacks of layers were considered in the calculations, without any roughness or imperfections. Some optical constants were estimated using room temperature values, which is not the case for real PLD or CVD depositions where elevated temperatures (~600-800 °C) are typically used. Similarly, the dielectric constants of TMDCs are currently not available, so they had to be estimated as well. Lastly, we assumed that the dielectric constants for $MoSe_2$ do not change with the number of layers, which to the best of our knowledge has not been studied yet. Consequently, the calculated dependences should only serve as a guide, and should find the most applicability for each material system once calibrated with *ex situ* TEM or other morphological analysis, like atomic force microscopy. In this case, as demonstrated here for PLD, a comparison between predicted and observed optical reflectivity should allow fundamental understanding and control over nucleation and growth processes.

Specular, single-wavelength laser reflectivity is easily implemented and should prove extremely important not only for routine use in online process diagnostics, but to reveal key kinetic phenomena. *In situ* reflectivity is extremely sensitive to reveal the nucleation stage and submonolayer growth kinetics where detection by other techniques such as Raman scattering and AFM are extremely challenging (as shown in Figs. S2 and S3 of the SI). This sensitivity allows precise determination of nucleation thresholds under different growth conditions. In general, the sensitivity of the technique appears capable of revealing how different processing parameters, such as reactant flux and kinetic energies at a given temperature, can be used to understand and tailor both nucleation and growth regimes. For the constant 1 Hz PLD conditions of these experiments, the initial kinetics could be described by a sigmoidal curve corresponding to nucleation-limited

autocatalytic kinetics, however, the digital delivery and *in situ* monitoring using this technique allows the adjustment of deposition parameters on-the-fly to follow a prescribed kinetic pathway.

The optical reflectivity signal contains fast temporal information for every laser pulse that may be coupled with faster observations of the pulsed deposition process (e.g., by plume photography and digitized ion currents) to understand processes such as subsequent desorption (e.g., residency time of Se deposited at higher temperatures, not shown), crystallization, or phase changes. Therefore, correlating the deposition information and control afforded by fast time-resolved reflectivity with the development of other *in situ* diagnostics such as Raman spectroscopy and second harmonic generation (that are typically employed for *ex situ* analysis of 2D materials) should form a powerful suite of optical tools to allow the correlation between evolving structure during synthesis and functionality of atomically-thin quantum materials.

Methods

$MoSe_2$ growth by PLD

A pulsed KrF (248 nm, 25ns FWHM, 1-50 Hz repetition rate) laser was used for the ablation of the targets in vacuum and argon background gas. A 1 in.-diameter $MoSe_2$ pellet (Testbourne Ltd, 99.9% purity) was used as the ablation target. Using a projection beamline, an aperture was imaged onto the target to produce a 1.3 mm x 4.5 mm rectangular spot. 50 mJ of laser energy was used, providing ~ 0.9 J/cm^2 per laser pulse at the target surface. SiO_2/Si substrates (typical size 1cm x1cm) with different thickness of the SiO_2 layer (University Wafer, Inc.) were adhered onto a 1 in. diameter heater (HeatWave Laboratories, Inc.) with a thin conductive silver paint. SiN TEM grids used for STEM measurements were attached to the substrates using tiny droplets of a silver paint. The substrate was placed 5 cm away from the $MoSe_2$ target in a cylindrical stainless-steel

chamber (50 cm inner diameter, 36 cm tall, Fig. S6a). The heater temperature was controlled to ± 2 °C via a PID controller, and ramp up and cooling rates were 30 °C/min. The growth was performed at 600 °C at a base pressure of 5.0 x 10^{-6} Torr.

Time-resolved reflectivity measurements

The transient growth of $MoSe_2$ was recorded using a HeNe laser (25-LHP-171-249, CVI Melles Griot, λ = 632.8 nm, 7 mW) reflected from the SiO_2/Si substrate. The HeNe laser beam passed through a neutral density filter and a 1-in. achromatic depolarizer (DPP25-A, Thorlabs Inc.) to randomize the polarization of the linearly polarized incident laser beam and was directed to the SiO_2/Si substrate at an incident angle of 78° (Figs. S6(b)-6(d)). The intensity of the specularly reflected beam from the substrate was recorded with a Si photodiode (SM1PD1A, Thorlabs) equipped with a narrow band 633nm interference filter and a LabView interfaced Keithley 2400 SourceMeter that recorded the photocurrent at 7 samples per second. The HeNe laser spot on the substrate has an elliptical shape (see Fig. S6d) and its size can be estimated based on the specified laser beam diameter (1.02 mm) and divergency (0.79 mrad) at $1/e^2$ as 1.6 mm x 6.5 mm.

Acknowledgements

The material growth, *in situ* diagnostics, and *ex situ* structural and optical characterizations were supported by the U.S. Department of Energy (DOE), Office of Science, Basic Energy Sciences (BES), Materials Sciences and Engineering Division. Research conducted at Oak Ridge National Laboratory's Center for Nanophase Materials Sciences (CNMS) which is a Department of Energy Office of Science User facility.

Supporting Information

The supporting information contains the following seven sections: S1, Calculation of optical reflectivity; S2, Atomic resolution STEM analysis; S3, Raman spectroscopy; S4, Atomic force

microscopy (AFM); S5, Gated ICCD imaging of laser ablation plume; S6. Modeling of growth kinetics; S7, Deposition rate.

Author contributions

DBG conceived and designed this work. AAP and DBG wrote the paper. AAP performed reflectivity calculations and kinetic modeling. YCL, AMS, SC, CMR conducted PLD experiments. GD, CL, YY, KX provided samples characterization. All the authors discussed the results and revised the paper.

References

1. M. Yamamoto and T. Namioka, In situ ellipsometric study of optical properties of ultrathin films, *Appl. Opt*. **31**, 1612-1621 (1992).

2. E. Langereis, S.B.S. Heil, M.C.M. van de Sanden, and W.M.M. Kessels, In situ spectroscopic ellipsometry study on the growth of ultrathin TiN films by plasma-assisted atomic layer deposition, *J. Appl. Phys*. **100**, 023534 (2006).

3. E. Langereis, S.B.S Heil, H.C.M. Knoops, W. Keuning, M.C.M. van de Sanden and W.M.M. Kessels, In situ spectroscopic ellipsometry as a versatile tool for studying atomic layer deposition, *J. Phys. D: Appl. Phys.* **42**, 073001 (2009).

4. M. Mahjouri-Samani, R. Gresback, M. Tian, K. Wang, A.A. Puretzky, C.M. Rouleau, G. Eres, I.N. Ivanov, K. Xiao, M. McGuire, Pulsed laser deposition of photoresponsive two-dimensional GaSe nanosheet networks, *Adv. Funct. Mater.* **24**, 6365-6371 (2014).

5. D.H. Lowndes, , D.B. Geohegan, A.A. Puretzky, D.P. Norton, C.M. Rouleau, Synthesis of novel thin-film materials by pulsed laser deposition, *Science* **273**, 898-903 (1996).

6. M. Mahjouri-Samani, M. Tian, A.A. Puretzky, M. Chi, K. Wang, G. Duscher, C.M. Rouleau, G. Eres, M. Yoon, J.C. Lasseter, K. Xiao, and D.B. Geohegan, Nonequilibrium synthesis of TiO_2 nanoparticle "building blocks" for crystal growth by sequential attachment in pulsed laser deposition, *Nano Lett.* **17**, 4624-4633 (2017).

7. C.N. Afonso, F. Vega, J. Gonzalo, C. Zaldo, Lithium niobate films grown by excimer laser deposition, *App. Surf. Sci.* **69**, 149 (1993).

8. R. Jordan, M. McConnell and J.G. Lunney, "*In situ* optical monitoring of pulsed laser deposition of $YBa_2Cu_3O_x$, *Supercond. Sci. Technol.* **8**, 504 (1995).

9. C.N. Afonso, J.M. Ballesteros, J. Gonzalo, G.C. Righini, S. Pelli, Rare-earth doped glass waveguides prepared by pulsed laser deposition, *App. Surf. Sci.* **96-98**, 760 (1996).

10. R. Serna, C.N. Afonso, In situ growth of optically active erbium doped Al_2O_3 thin films by pulsed laser deposition, *Appl. Phys. Lett.* **69**, 1541 (1996).

11. D. O._Mahony, J.G. Lunney, G. Tobin, E. McGlynn, Pulsed laser deposition of manganese doped GaN thin films, *Solid-State Electronics* **47**, 533 (2003).

12. D.B. Geohegan, A.A. Puretzky, I.N. Ivanov, S. Jesse, G. Eres, In situ growth rate measurements and length control during chemical vapor deposition of vertically aligned multiwall carbon nanotubes, *Appl. Phys. Lett.* **83**, 1851 (2003).

13. A.A. Puretzky, D.B. Geohegan, S. Jesse, I.N. Ivanov, G. Eres, In situ measurements and modeling of carbon nanotube array growth kinetics during chemical vapor deposition, *Appl. Phys. A* **81**, 223 (2005).

14. D.B. Geohegan, A.A. Puretzky, J.J. Jackson, C.M. Rouleau, G. Eres, and K.L. More, Flux-dependent growth kinetics and diameter selectivity in single-wall carbon nanotube arrays, *ACS Nano* **5**, 8311 (2011).

15. A.A. Puretzky, D.B. Geohegan, J.J. Jackson, S. Pannala, G. Eres, C.M. Rouleau, K.L. More, N. Thonnard, and J.D. Readle, Incremental growth of short SWNT arrays by pulsed chemical vapor deposition, *Small* **8**, 1534 (2012).

16. J.J. Jackson, A.A. Puretzky, K.L. More, C.M. Rouleau, G. Eres, and D.B. Geohegan, Pulsed growth of vertically aligned nanotube arrays with variable density, *ACS Nano* **4**, 7573 (2010).

17. A. A. Puretzky, D.B. Geohegan, S. Pannala, C.M. Rouleau, M. Regmi, N. Thonnard, G. Eres, Real-time optical diagnostics of graphene growth induced by pulsed chemical vapor deposition, *Nanoscale*, **5**, 6507 (2013).

18. A.A. Puretzky, I. Merkulov, C.M. Rouleau, G. Eres, and D.B. Geohegan, Revealing the surface and bulk regimes of isothermal graphene nucleation and growth on Ni with in situ kinetic measurements and modeling, *Carbon* **79**, 256 (2014).

19. Z.H. Ni, H.M. Wang, J. Kasim, H.M. Fan, T. Yu, Y.H. Wu, Y.P. Feng, Z.X. Shen, Graphene thickness determination using reflection and contrast spectroscopy, *Nano Lett*. **7**, 2758 (2007).

20. A. Hutzler, C. D. Matthus, M. Rommel, and L. Frey, Generalized approach to design multi-layer stacks for enhanced optical detectability of ultrathin layers, *Appl. Phys. Lett.* **110**, 021909 (2017).

21. I. Jung, M. Pelton, R. Piner, D.A. Dikin, S. Stankovich, S. Watcharotone, M. Hausner, R.S. Ruoff, Simple approach for high-contrast optical imaging and characterization of graphene-based sheets, *Nano Lett.* **7**, 3569 (2007).

22. S. Roddaro, P. Pingue, V. Piazza, V. Pellegrini, F. Beltram, The optical visibility of graphene: interference colors of ultrathin graphite on SiO_2, *Nano Lett*. **7**, 2707 (2007).

23. D.S.L. Abergel, A. Russell, V.I. Fal'ko Visibility of graphene flakes on a dielectric substrate, *Appl. Phys. Lett*. **91**, 063125 (2007).

24. W. Lu, H. Nan, J. Hong, Y. Chen, C. Zhu, Z. Liang, X. Ma, Z. Ni, C. Jin, Z. Zhang, Plasma-assisted fabrication of monolayer phosphorene and its Raman characterization, *Nano Res.* **7**, 853 (2014).

25. H. Chen, W. Fei, J. Zhou, C. Miao, W. Guo, Layer identification of colorful black phosphorus, *Small* **13**, 1602336 (2017).

26. A. Castellanos-Gomez, N. Agraït, G. Rubio-Bollinger, Optical identification of atomically thin dichalcogenide crystals, *Appl. Phys. Lett.* **96**, 213116 (2010).

27. Y. Li, N. Dong, S. Zhang, K. Wang, L. Zhang, J. Wang, Optical identification of layered MoS_2 via the characteristic matrix method, *Nanoscale* **8** 1210 (2016).

28. D. Bing, Y. Wang, J. Bai, R. Du, G. Wu, L. Liu, Optical contrast for identifying the thickness of two-dimensional materials, *Opt. Comm.*, **406** 128 (2018).

29. O.S. Heavens, Optical properties of thin solid films, Dower Publications, Inc., New York, 1991. Originally published: London, England: Butterworths Scientific Publications, 1955.

30. Y. Li, A. Chernikov, X. Zhang, A. Rigosi, H.M. Hill, A.M. van der Zande, D.A. Chenet, E. M. Shih, J. Hone, T.F. Heinz, Measurement of the optical dielectric function of monolayer transition-metal dichalcogenides: MoS_2, $MoSe_2$, WS_2, andWSe_2, *Phys. Rev. B* **90**, 205422 (2014).

31. G.E. Jellison, Jr., F.A. Modine, Optical functions of silicon at elevated temperatures, *J. Appl. Phys.* **76**, 3758 (1994).

32. G. Eres, M. Regmi, C.M. Rouleau, J. Chen, I.N. Ivanov, A.A. Puretzky, D.B. Geohegan, Cooperative island growth of large-area single-crystal graphene on copper using chemical vapor deposition, *ACS Nano* **8**, 5657 (2014).